

Article

# Concrete CFRP-Reinforced Beam Performances, Tests and Simulations

Christiana Emilia Cazacu<sup>1</sup>, Cristian Ștefan Dumitriu<sup>2,\*</sup>  and Alina Bărbulescu<sup>1,\*</sup> 

<sup>1</sup> Department of Civil Engineering, Transilvania University of Brasov, 5 Turnului Str., 500152 Brasov, Romania; christiana.cazacu@unitbv.ro

<sup>2</sup> Department of Mechanical Engineering and Robotics in Constructions, Technical University Civil Engineering Bucharest, 56 Plevnei Av., 500152 Bucharest, Romania

\* Correspondence: cristian.dumitriu@utcb.ro (C.Ș.D.); alina.barbulescu@unitbv.ro (A.B.)

**Abstract:** Nowadays, the increasing necessity of consolidating and renewing buildings represents a big challenge for engineers. Structural consolidation using composite materials glued on the damaged surface using high-performance adhesives could be a viable technical solution. In this context, this article's aim is twofold. First, it presents the experimental results of the investigations performed on three types of reinforced concrete (RC) beams—without consolidation (G1), consolidated with carbon fibre-reinforced polymer (CFRP) lamella of SikaCarboDur (G2), and consolidated with CFRP fabrics (G3)—to determine their behavior under different loads. Second, a numerical study was performed using Finite Element Analysis (FEA) to compare and confirm the experimental results (stress, displacement). The numerical simulation shows that the stress in the areas covered by wraps is approximately 20% lower than in those without wraps.

**Keywords:** concrete beam; consolidation; CFRP; strengthening; FEA



**Citation:** Cazacu, C.E.; Dumitriu, C.Ș.; Bărbulescu, A. Concrete CFRP-Reinforced Beam Performances, Tests and Simulations. *Sustainability* **2024**, *16*, 2614. <https://doi.org/10.3390/su16072614>

Academic Editor: Constantin Chalioris

Received: 5 February 2024

Revised: 13 March 2024

Accepted: 21 March 2024

Published: 22 March 2024



**Copyright:** © 2024 by the authors. Licensee MDPI, Basel, Switzerland. This article is an open access article distributed under the terms and conditions of the Creative Commons Attribution (CC BY) license (<https://creativecommons.org/licenses/by/4.0/>).

## 1. Introduction

Fiber-reinforced plastic (FRP) products were first used to reinforce concrete structures in the mid-1950s [1]. Urs Meier and his colleagues developed and applied CFRP in the construction industry. In their lamellar form, CFRPs were first operated in 1991 to renovate the Ibach Bridge (Lucerne) [2]. In 1999, a carbon fiber polymer lamellar material was developed by EMPA and marketed by SIKA. Since then, these materials have been utilized to consolidate or rehabilitate hundreds of buildings, bridges, or structural elements [3–9]. Therefore, many standards and regulations have been implemented worldwide for applying and using FRP composite materials [10–17].

Many studies have explored CFRP's behavior and practical applications for repairing concrete construction elements subject to mechanical wear or deterioration due to long-term exploitation.

The first group of approaches contains the experimental research of the CFRP-RC beams in different scenarios [18,19]. Other studies have provided combined experimental and numerical analyses [20–23]. For example, Zhong et al. [20] studied crack propagation in RC structures using a three-phase concrete model. Arduini and Nanni [21] analyzed the behavior of pre-cracked RC beams strengthened with CFRP sheets. It was shown that strengthening was significant, but the effect on different monitored variables was insignificant. The crack propagation in concrete on pre-cracked beams under various loading rates was performed by Bu et al. [22] using the digital image correlation method.

Another article category focuses on forecasting the deflection of RC beams [24–26] or building analytical models for RC beams [27–29]. A model for the crack propagation at the CFRP–concrete interface under fatigue loading is presented in [30].

Only a few articles contain simulations of RC beams reinforced with CFRP, among which we mention those of Uz et al. [31] with Abacus, Al-Jasmi et al. [32], and Carvalho

Silva [33] with Ansys. The studies in [34,35] provide a state-of-the-art review of the behavior and strength of FRP-strengthened RC structures.

Monitoring the beams' behavior under different loadings and investigating damage using non-destructive evaluation techniques (NDTs) is a critical study topic [36–41]. NDTs were categorized into five groups [41]: (1) visual inspection [41]; (2) acoustic wave-based techniques [36], like acoustic emission (AE) [36,42], impact-echo [36,41,42], ultrasonic testing [40], and acoustic-laser techniques [42]; (3) optical techniques like infrared thermography, digital shearography [43] and terahertz testing; (4) imaging-based techniques like microwave NDTs [44], (5) electromagnetic methods like magnetic resonance [45], and electro-mechanical impedance [37]. Data fusion [38] is also utilized because it combines data from different sources.

NDTs can scatter the material's microstructure fracture energy, which is important for understanding the crack path during the damage distribution in the fracture's surface [46]. AE techniques can detect the sudden energy release associated with crack formation or growth [47]. The acoustic emission moment tensor analysis can identify the crack type, its orientation, and kinematics. A detailed presentation of NDTs may be found in [48–50], and reviews of different applications in [41,51].

Using composite materials in the construction field over the last decade has also led to the development of theories that explain the composite's mechanical behavior and adopt finite element software for their analysis. In the international context of reducing waste and using cleaner technologies, this study aims to analyze the application of CFRP-type composite materials on RC structural elements. Therefore, the main objective of this study is to test the hypothesis that reinforcing concrete beams with CFRP increases the elements' strength and shape stability.

With respect to the existing literature, the novelty of our approach consists of numerical simulation, with SolidWorks, of the mechanical behavior of the reinforced beams with CFRP lamella and wraps. Computation of the stress intensity in the regions covered by the CFRP wraps and without wraps was performed. The results show that the stress in the zones protected with CFRP wraps is lower than in the unprotected ones. Therefore, the covered areas are less susceptible to the cracks' apparition and propagation. The same conclusion was drawn after visual observation of the cracks on the beams during the experimental study.

## 2. Materials and Methods

### 2.1. Experiments

The experimental program consisted of stressing three steel RC beams with a concentrated force (P) applied in their middle. The beams had a cross-section of 15 cm × 20 cm and a length of 100 cm. The hydraulic machine used in the experiments was composed of two supporting steel rollers and an upper roller supported by a transverse articulated arm. The rollers had a circular cross-section with a diameter of 20 mm and 10 mm longer than the width of the test specimen. The loading was progressively increased from zero until the beam failure, with a variation rate of 5 kN/s. The experimental setup is presented in Figure 1 [52]. Fabrication, surface treatments, and testing were performed under ambient laboratory conditions (20 °C and normal relative humidity) [53–56].

The experiments were conducted according to the EN 12390-5:2019 standard *Test on hardened concrete. Part 5: Flexural strength of specimens* [57]. The purpose of the experiments includes [52]:

- Tracking the final displacement value for each type of beam tested.
- Building of characteristic unitary force–displacement diagrams.
- Determining the bearing capacity changes of beams provided with CFRP fabrics or lamella.

The concrete used for the beam fabrication was of heavy type, ordinary class, C16/20, according to NE-012/1-2010 [58]. The calculation of the recipe according to which the

concrete was prepared complies with the provisions of SR EN 206-1:2002 [59]. For 1 m<sup>3</sup>, the following quantities were utilized:

- Dry aggregate 0–4 mm—770 kg (46%);
- Dry aggregate 4–8 mm—335 kg (20%);
- Dry aggregate 8–16 mm—570 kg (34%);
- Cement type CEM II/A-S 42, 5R—355 kg;
- Water—230 kg;
- Additive type BV3M—2.84 L.



**Figure 1.** The experimental setup and a sample before starting the experiment [52].

C16/20 Concrete Design Properties according to EN1992-1-1: characteristic cylinder compressive strength,  $f_{ck} = 16$  MPa and characteristic cube compressive strength,  $f_{ck,cube} = 20$  MPa. The strength classes of EN1992-1-1 are based on the characteristic strength classes determined at 28 days.

The aggregates were weighed dry to calculate the recipe using standardized methods. The corrections of the granularity curve of the total aggregate and apparent concrete density were carried out. The beams were cast in optimal conditions in special formwork, removed from the formwork after 24 h, and kept in a humid environment for 28 days after casting.

The steel reinforcement scheme is presented in Figure 2 and consists in:

- Two OB 37 (S235) steel bars, with a diameter of 6 mm, on the upper part;
- Two OB 37 (S235) steel bars, with a diameter of 6 mm, and the lower part;
- 23 transverse stirrups OB 37 (S235) steel bars.

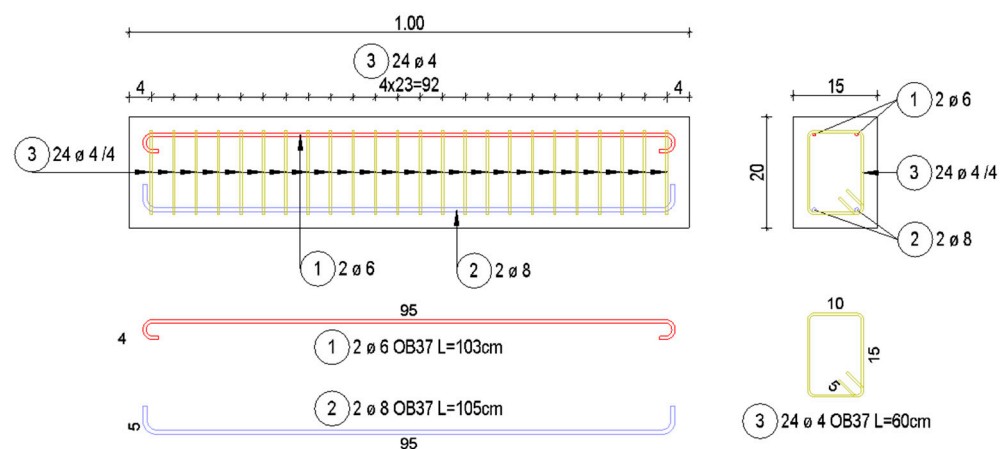


**Figure 2.** The steel and section's details.

Technical details of concrete steel OB37 with a smooth profile are the following, according to Romanian STAS 438-1:2012:

- Symbolization: O—steel; B—concrete; number 37—ultimate tensile strength (370 MPa).
- Steel chemical composition: C—0.230%; Mn—0.750%; P—0.045%, S—0.045%, Si—0.400%; Ni—0.300%; Cr—0.300%; Cu—0.500%.
- Mechanical properties: yield strength—min. 235 MPa and tensile load—min. 360 MPa; elongation (A)—min. 25%.

The CFRP materials utilized are (1) SikaWrap-230C [60], together with SikaDur-330 epoxy resins [61], and (2) SikaCarboDur S blades [62], together with SikaDur-30 adhesive [63]. The mechanical characteristics of the CFRP are presented in Table 1.

**Table 1.** Mechanical characteristics of the materials.

CFRP	Tensile Strength (MPa)	Elasticity Module (MPa)	Thickness (mm)	Elongation (%)
SikaWrap-230C	3200	220,000	0.129	1.56
SikaCarboDur S 512	2800	160,000	1.2	1.69

Note that on a properly prepared concrete surface, the adhesion force is greater than the concrete's yield strength,  $4 \text{ N/mm}^2$ , and the modulus of elasticity is  $12,800 \text{ N/mm}^2$ .

The research was developed in two directions to emphasize the effect of using CFRP for RC beams. The first studied the decrease of the stress intensity in concrete beams subjected to flexural stress. The second aimed to determine restoration solutions for the load-bearing capacity of non-critical damaged beams using composite materials bonded to them. This paper presents the results of the first research direction, which are the basis of the numerical analysis developed as a solution for similar future studies that can be performed without experimental tests.

Three beams of the same size and steel reinforcing were tested for flexural stress:

- A standard beam, G1 (Figure 3), which is the reference beam.
- A beam G2, which is a G1 beam provided with one CFRP lamella of SikaCarboDur type S 512, with dimensions  $800 \text{ mm} \times 50 \text{ mm} \times 1.2 \text{ mm}$ . The lamella is glued to the bottom of the beams with SikaDur-30 adhesive, as in Figure 4(left).
- A beam G3, which is a G1 beam provided with "U"-shaped CFRP fabrics made of SikaWrap-230C and glued with SikaDur-330. The fabrics are 150 mm wide and cover the beam's bottom and sides, slightly overlapping its top. The distance between fabrics is 100 mm, as in Figure 5.

The loading force at which the first cracks appeared, the maximum breaking force at which the beam or the composite material yielded, and the maximum deflection at the moment of beam failure were measured during the laboratory tests. The device with which the tests were carried out recorded the P forces' values. A special magnifying glass was used to measure the cracks and openings. The deflection was measured using a device with an analog comparator (0.01 mm resolution) placed between the test beam and the testing machine support plate.

The test was developed for static load analysis. A specific extended study will be performed for the dynamic analysis.

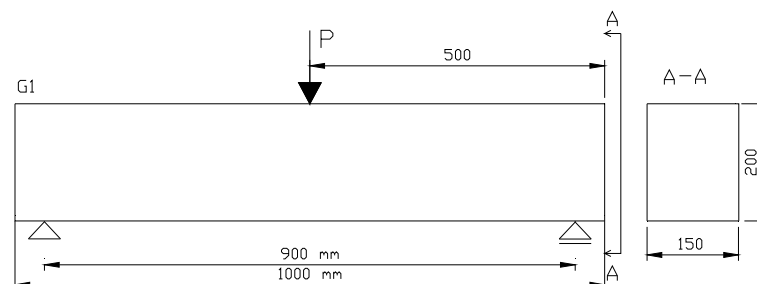


**Figure 3.** G1 beam.

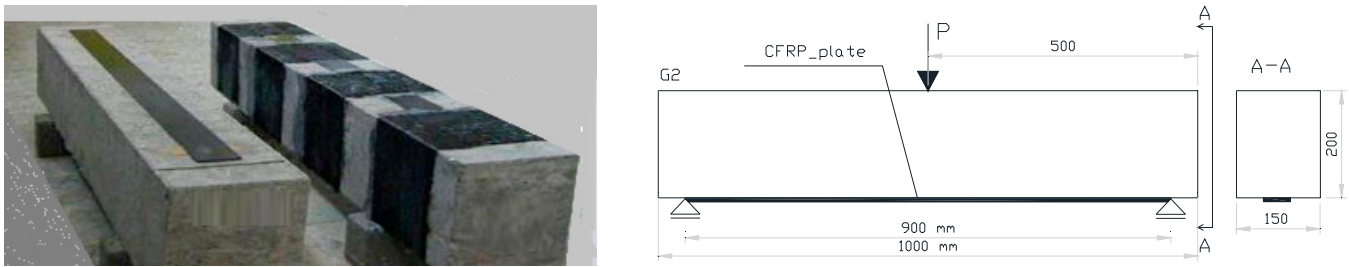


**Figure 4.** (left) G2 beam with lamella and wrap; (right) scheme of a beam with lamella.

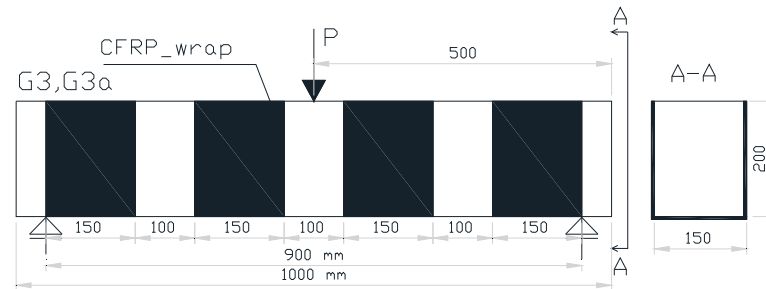


**Figure 5.** The model of the G3 beam.

## 2.2. Simulation

In most cases, concrete-based structures are designed using specialized construction software. The rules and regulations based on experimental research and practice, like EN 1992-1-1: 2004 Eurocode 2: Design of the concrete structures [64], form the background of such an approach. When performing research, employing FEA is the only solution to accurately predict the structure's response to thermal or mechanical stresses. Therefore, the second part of the article presents the simulation for the beams G1–G3 using SolidWorks Simulation 2022 software [65]. The results should reflect the differences in the mechanical properties of the analyzed beams, G1, G2, and G3, and validate the experiments in some representative stages.

Another simulation was performed for a beam named G3cw to determine whether the simulation could assist in designing CFRP-CR beams (as in the experiments described in Section 2.2). G3cw was designed based on G3 using the same type of wraps, replacing the four meshes (Figure 5) with three, one in the center and the other two symmetrically at a 100 mm distance.

Using SolidWorks is appropriate because the study aims to determine the influence of the CFRP reinforcement on concrete resistance and stability without considering the cracks. For this aim, we studied the following parameters: stress intensity, displacement, and Factor of Safety. The SolidWorks Simulation software has no Cracks Plot module implemented, so the concrete crack initiation and propagation simulation is impossible. Despite this drawback, the simulation can be performed to compute the stress, deflection, Factor of Safety, reaction forces, etc. for the linear-elastic concrete behavior. These results will be presented in the following sections.

According to the material resistance theories, this study's proper method for the Factor of Safety (FOS) calculus is the Mohr–Coulomb theory, also known as the Internal Friction theory. This failure criterion is used for brittle materials with different tensile and compressive properties, such as concrete or CFRP materials, which do not have a specific yield point. Consequently, using the yield strength to define the limit stress for this criterion is not recommended.

The Mohr–Coulomb theory predicts failure when combining the maximum tensile principal stress and the minimum compressive principal stress exceed their respective stress limits. This criterion is implemented in SolidWorks Simulation software and was used in this research for the FOS Plots [66].

For the Stress Plots (the display of the computed stress), SolidWorks uses the following methods: 1st, 2nd, or 3rd Principal Stress (P1, P2 or P3), von Mises Stress, Stress Intensity (P1–P3) (Tresca) and Triaxial Stress (P1 + P2 + P3), where P1, P2, and P3 represent the stress calculated for the principal axes. This article applied the Stress Intensity plot instead of the von Mises Stress plot because it is more appropriate for brittle materials.

The maximum shear stress theory shows that a material failure occurs when the absolute maximum shear stress has a value that causes the material to yield in a simple tension test [67]. This criterion satisfactorily covers all materials used in the experiments: concrete, steel, and CFRP, including the bonding adhesive.

Usually, simulation validation is performed by comparison with the experimental results and is well applied to ductile materials. The simulation and experiments on structures with combined materials—ductile and brittle—are the most difficult to perform and, consequently, to validate. Our search through the scientific literature found no recommended methodology to validate the simulation, no matter what software was used. Therefore, all the input data (model dimensions, materials' characteristics, constraints, loadings, and component interaction) were double-checked in the preprocessing stage. Finally, setting the appropriate FEA solver, computational parameters, and failure criterion based on the software error handling capabilities will ensure computational accuracy.

### 3. Results and Discussion

#### 3.1. Experimental Results

The characteristic force–displacement diagram for the tested beams is presented in Figure 6.

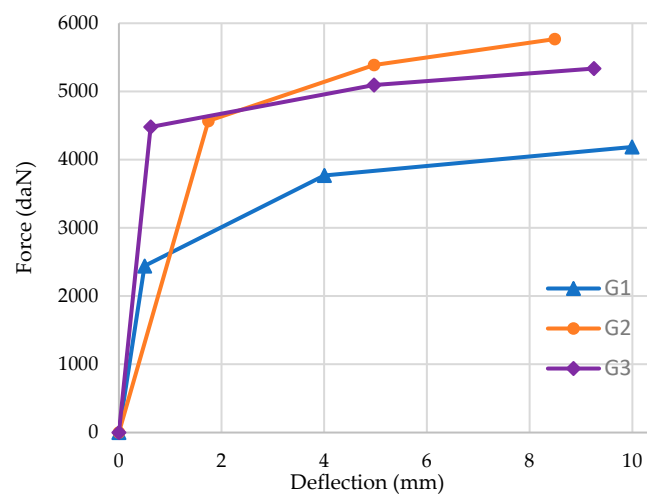


**Figure 6.** The characteristic force–displacement diagrams for G1, G2, and G3.

The following aspects result from studying and comparing the specific characteristic force–displacement diagrams obtained for each beam type.

- The diagrams are trilinear, highlighting the three working stages of RC elements. The limit of the working stage I corresponds to the situation when the loads are low. The entire RC section is active and behaves like a linear elastic material. The unit effort value corresponds to 40–50% of the yield strength value.
- Continuing loading after the first cracks' apparition suddenly increases the unit efforts in the compressed concrete and tensioned reinforcement.
- In the normal sections, the resistance limit state corresponds to the stage II limit and approximately 80% of the breaking moment.
- Increasing the loading increases the specific deformations and unitary efforts. Finally, the second stage's limit is reached when a material (steel reinforcement, concrete, or

carbon material) reaches the ultimate specific deformations, triggering the breaking process and passing to the third stage.

- In the third stage of work, the beams fail due to the crushing of the compressed concrete and the irreversible span of the cracks in the beam's stretching area.

Figure 6 shows the effect of applying CFRP on the beams' surface. The resistance of the consolidated beams G2 and G3 is significantly higher compared to the reference beam G1. When studying the characteristics of the two materials (fabrics and lamella), one would expect a better resistance by applying the last one. The experiment demonstrates that the obtained results are similar for lamella and fabrics from the viewpoint of deflection and maximum force applied. What makes the difference between the consolidation solution is the behavior and failure way of the consolidated element. The G2-type beam yielded suddenly and without warning following the detachment of the lamella. The G3-type beam behaved similarly to the reference beam, the deformations being proportional to the load, and the failure moment was predictable.

The results concord with the theory that indicates that during the first stage, the deflection increases until vertical cracks open in the cross-section tensioned part; then, in stage 2, it increases until the yielding strength of the tensioned reinforcement is reached. In the last stage, the yielding reinforcement strength is reached, and the tensile force is intercepted by CFRP [68]. Moreover, *'the stress-strain curve for concrete is approximately linearly elastic up to the maximum tensile strength in tension. After this point, the concrete cracks and the strength decreases gradually'* [69,70].

Figure 7 displays images taken with the beams and the apparatus used during the experiments (the apparition of the cracks in G1 and G2). Table 2 contains the force values at the apparition of the first cracks (P) and at breaking (F), as well as the corresponding beam deflection. More pictures taken during the experiments are shown in [52,54–56].



Figure 7. G1 (left), and G2 (right).

Table 2. The force at the apparition of the first cracks, the breaking force, and the beams' deflections.

Beam Type	Force at the Apparition of First Cracks (P)	Breaking Force (F)	Beam Deflection
G1	23.5 kN	39.0 kN	7.5 mm
G2	28.5 kN	54.5 kN	5.0 mm
G3	40.0 kN	51.0 kN	5.0 mm

From Table 2, it is easy to observe how the different arrangements of CFRP materials influence the beam's behavior under load. For example, when the lamella was glued on the beam's bottom, the load of the G2 increased by 21% at the crack's initiation compared to the reference beam, G1. The application of CFRP led to better behavior under load. At the same applied force, unconsolidated beams showed cracks, but the cracks were not visible on the consolidated beams. Moreover, the consolidated beams did not have a noticeable deflection.

Applying composite materials reduced the consolidated element deflection under the load and the steel bars' specific deformations. The final value of the concentrated force also

increased. The unconsolidated beam G1 yielded under a force of 39 kN. After applying lamellas (G2), the breaking force increased by 40%. For the fabrics oriented parallel to the force (G3), it increased by 30%. The elastic behavior of the CFRP glued to the beams led to a high degree of elastic behavior of the beams in the second work stage. In some cases, even in the third work stage, a certain degree of elastic behavior was manifested because the remaining deformations (cracks) had values between  $L/600$  and  $L/750$ . Table 3 contains information about the cracks' span.

**Table 3.** Cracks span for G1, G2, and G3.

Beam Type	G1	G2	G3
Cracks span (mm)	5.5	2	5

At the end of the tests, the beams reinforced with fabrics showed cracks only in the central part and areas where CFRP was not applied. When the composite material was detached from the beam's surface, the fabrics came off with the concrete, and no damage to the concrete under the fabrics was noted (Figure 8) [55].

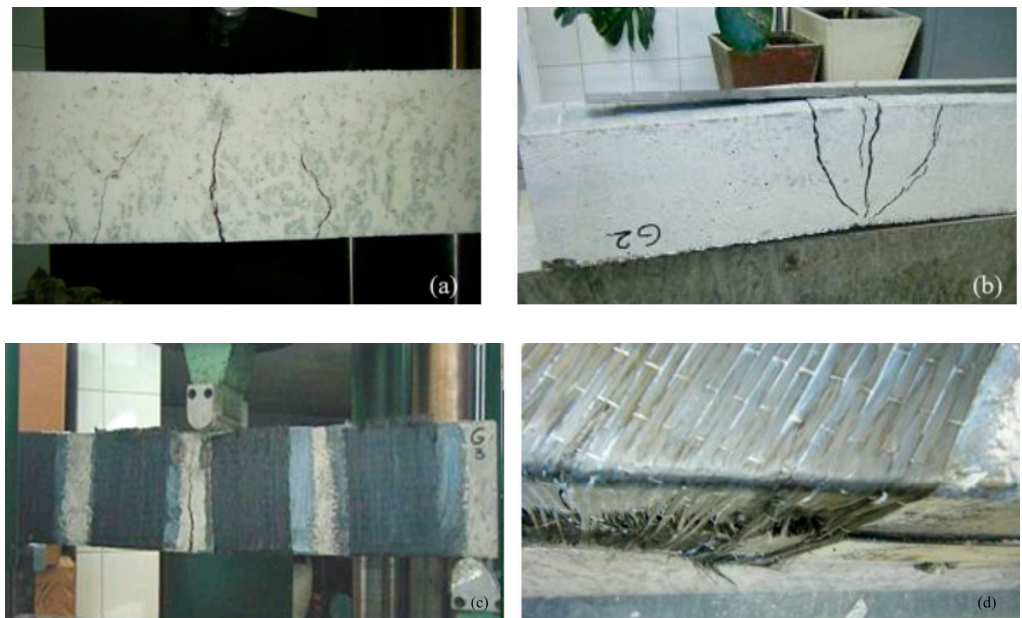


**Figure 8.** (a) Failure mode of G1; (b) failure mode of G2; (c) failure mode of G3 (d); wrap detached from the beam's surface.

More investigations must be performed with different positions of the wraps. Moreover, if wraps entirely cover the surface, other methods should be used to observe crack initiation and propagation.

Interestingly, however, the recorded values of the breaking force for G2 and G3 were almost equal. In the experiment, better values could be obtained for the beams reinforced with carbon lamellas if their detachment from the concrete surface would be avoided by anchoring them at the beam's ends. In all cases, the lamella detached from the concrete surface before reaching the maximum bearing capacity, leading to the sudden destruction of the entire element. The failure mode by breaking or detaching the carbon lamellae is unique and characteristic of RC elements or strengthened with such materials. This is due to the appearance of some crack planes inside the concrete element, the weak transverse strength, and the brittle behavior. The element failure suddenly occurs, almost without warning (as in the G2 case). From breaking or detaching the CFRP lamella, the concrete element deforms quickly, cracks appear and progress rapidly, and the entire element fails. When

fabrics cannot be applied, carbon blades can also be arranged, but they should be very well anchored or fastened with screws at the beam's ends to avoid their sudden detachment.

### 3.2. Numerical Study Using Finite Element Analysis

Numerical simulation has three steps:

- Preprocessing: the model is built with Computer-Aided Design (CAD) software ([https://www.autodesk.com.hk/solutions/cad-design#:~:text=Computer-aided%20design%20\(CAD\),done%20using%20pencil%20and%20paper](https://www.autodesk.com.hk/solutions/cad-design#:~:text=Computer-aided%20design%20(CAD),done%20using%20pencil%20and%20paper), accessed on 2 February 2024),
- Solving the finite element model: meshing the model, defining the constraints and loads, setting the boundary conditions, and solving the system of equations,
- Post-processing: plotting the desired results and performing the analysis of the results.

Computer Aided Engineering (CAE) software is necessary for the second and third steps. SolidWorks software integrates CAD and CAE modules, an important advantage in simulation research.

Figure 9 contains the representation of the beam numerical model in two phases. Figure 9 Left presents the model configuration, and Figure 9 Right includes the simulation setup. In the model configuration, the red cylinder is the cylinder on which the loading force is applied. The other two blue cylinders are intended to support the beam, the left one being fixed and the right mobile. The concrete beam in this figure is in the 'transparency on' mode that makes the interior steel bars visible.

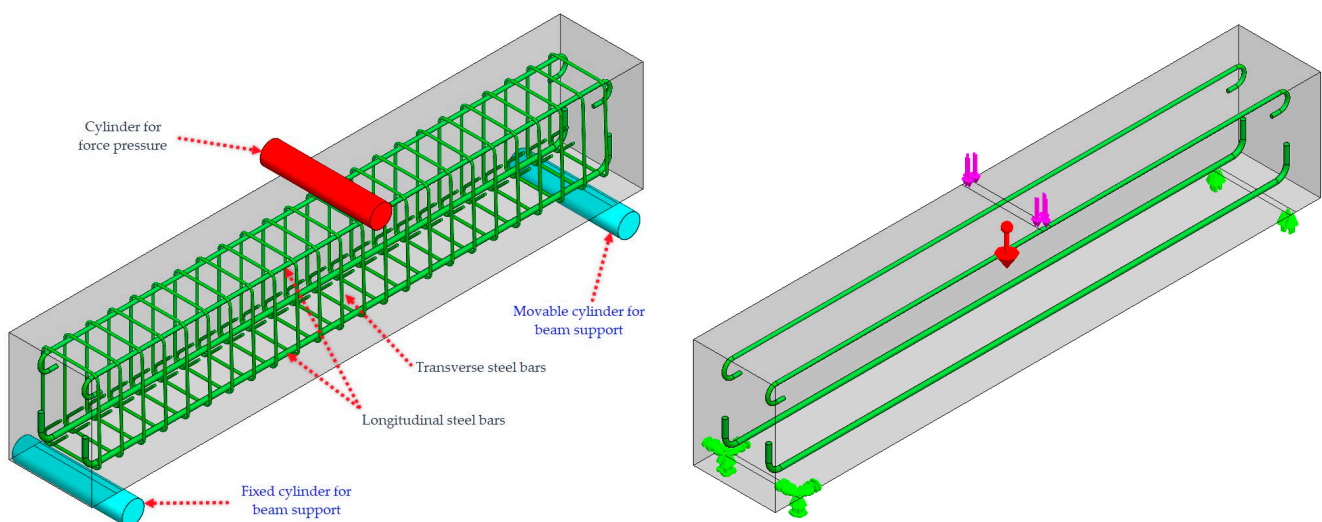


**Figure 9.** Numerical model: model configuration (left) and simulation setup (right).

In the simulation setup, Figure 9(right), the magenta arrows represent the loading force (replacing the red cylinder from Figure 9(left)), the left green arrows represent the fixed supporting points (three directions locked), and the right green arrows the slipping supporting points (the vertical direction locked). The red arrow represents the gravity force given by the mass of the simulated beam. The contact between the cylinder and the beam creates a 15 mm wide footprint in the case of the force cylinder and a 10 mm wide footprint in the case of the supporting ones.

The simulation model respects the dimensions of the tested beams. In the flexural load cases, the transverse elements from steel reinforcement beams have a very low influence due to the force direction and setup condition (horizontal beam position, vertical force). If those elements are ignored, the computation effort will dramatically decrease without affecting the results. The simplified model contains only the main bars.

The material's characteristics for the beam's reinforcing elements have been defined in the software for each designed part according to the values presented in Table 1. As the materials are considered brittle, the yield strength value is unavailable.

The discretization of the solid must be performed after building the model. The mesh is created using the ‘mesh control tool’ implemented in the software, which provides options to set the mesh parameters. The first step in the mesh generation starts with the default element size (which is set by the software according to the model). If the generation is not performed, the mesh parameters are set iteratively until all elements are entirely discretized. This model mesh succeeded with standard mesh for the element size = 10.87 mm and the ratio = 1.5 (ratio of the element size in one layer to the element size in the preceding layer), as shown in Figure 10.

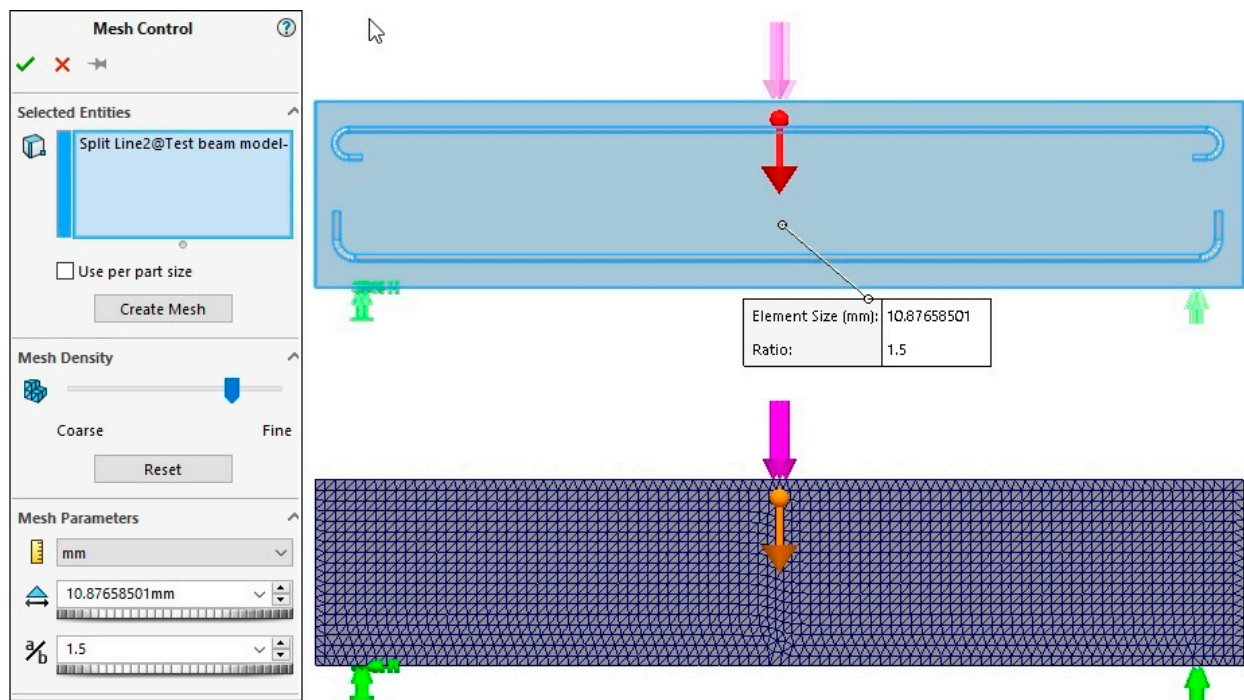


**Figure 10.** Mesh parameters' values and mesh plot.

The component interaction settings given for global interaction (all parts) are:

- Interaction type: bonded (this covers the weld and glue bound). The assembly components are meshed independently.
- Gap range for bonding: 0 mm.
- Bounding formulation: surface to surface (this option is more accurate but slower than node to surface).

This study was run using the FFEPlus solver, which employs advanced matrix reordering techniques to make it more efficient for large problems. The thermal influence was not considered, and the reference temperature at zero strain is 25 °C.

The presented stress values refer to the mesh elements instead of the mesh nodes as a better way to analyze the stress field.

In the simulations, the beams were statically stressed in two cases. A load of 23.5 kN (the force at which the first cracks appeared in G1) and 37.5 kN were applied in the first and second cases, respectively. The last value was chosen to be lower than the breaking force of G1 (39 kN).

The mechanical properties, maximum shear stress (Tresca) (MPa) displayed as intensity, and displacement (mm) were graphical and numerically plotted in both cases. The graphs obtained for the load of 23.5 kN are only presented, while those for 37.5 kN are similar because the simulations were performed in the same modeling conditions.

### 3.2.1. Simulation of the Beam G1 under the Load of 23.5 kN

Figure 11(left) presents the deformed shape of G1 together with the Stress Intensity plot. The highest stress, represented by red, appears in the contact areas of the three working cylinders (two at the bottom for support and one at the top for pressing).

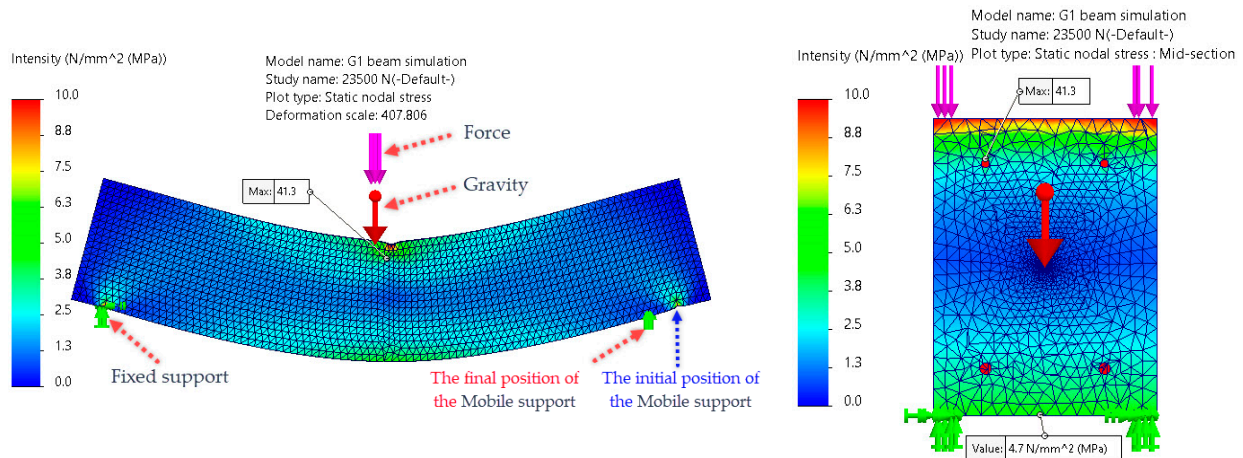


**Figure 11.** Deformed plot (left) and mid-section representation (right) of the stress intensity of G1 at 23.5 kN load.

The maximum stress intensity representation scale has been set to 10 MPa to better represent the high-stressed areas in color. The maximum stress value is 41.3 MPa, corresponding to the top reinforcement steel bars, as shown in Figure 11(right).

The red zones in the place of the top and bottom-right cylinders are shifted to the right, confirming that the beam slides slightly to the right on the rolling support during mechanical stress. In the graphical representation, the software keeps the application points for forces and supports in the same position and changes the beam's position according to the deformation intensity. The left support does not move because it is declared a fixed point. This situation appears in all other simulations.

The zone of interest for the present analysis is the middle point at the bottom of the beam, where the concrete elongation reaches its maximum value. The calculated stress at this point is 4.7 MPa. The existence of the red-colored zones on the top of the concrete was expected and confirms the high contact pressure between the force cylinder and the concrete surface. The highest displacement value is 0.25 mm (Figure 12(left)) on the beam top, where the concrete local deformations appear due to the contact pressure forces. Figure 12(right) presents the Factor of Safety (FOS) plot generated only for concrete.

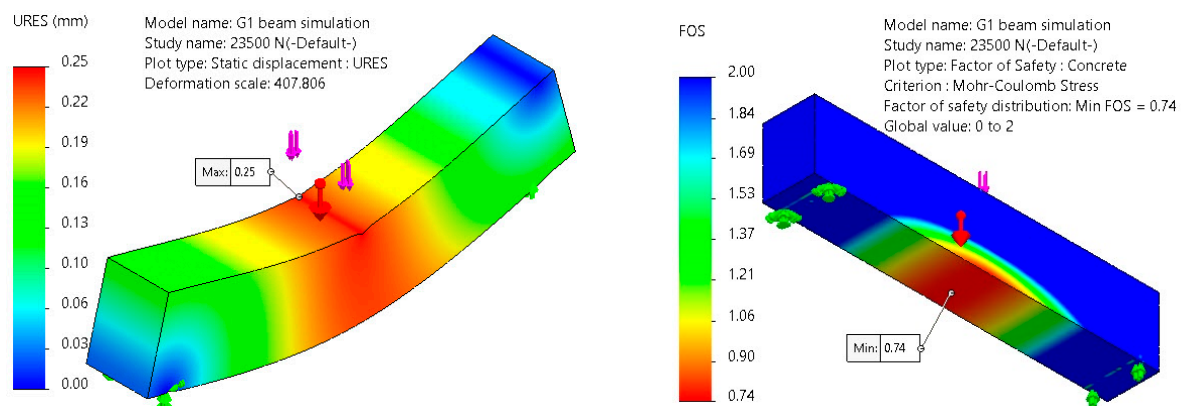


**Figure 12.** Deformed shape of the resultant displacement (URES) of G1 at 23.5 kN load (left). The FOS plot for the concrete on G1 at 23.5 kN load (right).

The failure criterion was changed to Mohr–Coulomb Stress, a better choice for brittle materials like concrete and stones. The minimum FOS =  $0.74 < 1$ , which confirms the crack initiation state, as in the experimental tests.

### 3.2.2. Simulation of the Beam G2 under the Load of 23.5 kN

The beam G2 is reinforced on the bottom face with a lamella Sika Carbodur S, type 512. Figure 13(left) shows the beam from the down-left to the top-right view. The lamella is almost entirely red because the stress intensity exceeded 10 MPa (the graphical set limit). Its body records a maximum stress intensity of 43.2 MPa.

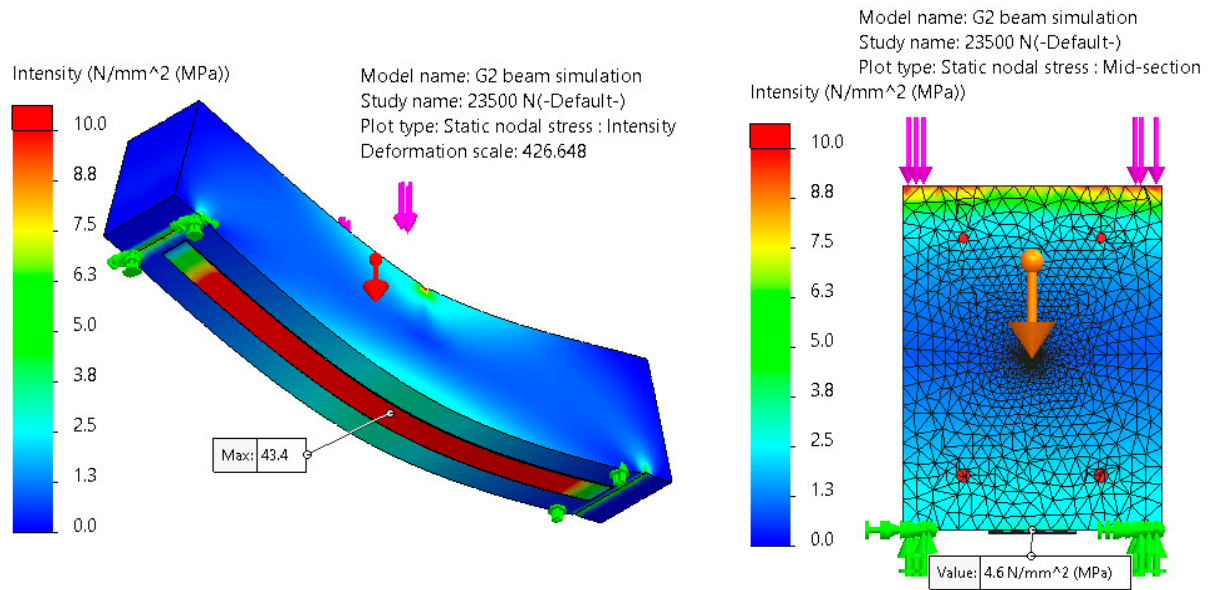


**Figure 13.** Deformed plot (left) and mid-section representation (right) of the stress intensity of G2 at 23.5 kN load.

The lamella takes over part of the mechanical load to the concrete beam benefit. Consequently, the concrete stress decreases from 4.7 MPa (Figure 11(right)) to 4.6 MPa (Figure 13(right)). The resultant displacement URES slightly decreases from 0.25 mm (Figure 12(left)) to 0.24 mm (Figure 14(left)), and the FOS slightly increases from 0.74 (Figure 12(right)) to 0.79 (Figure 14(right)). The FOS values increase from the outside to the center of the beam, where the elongation and compression are equal.

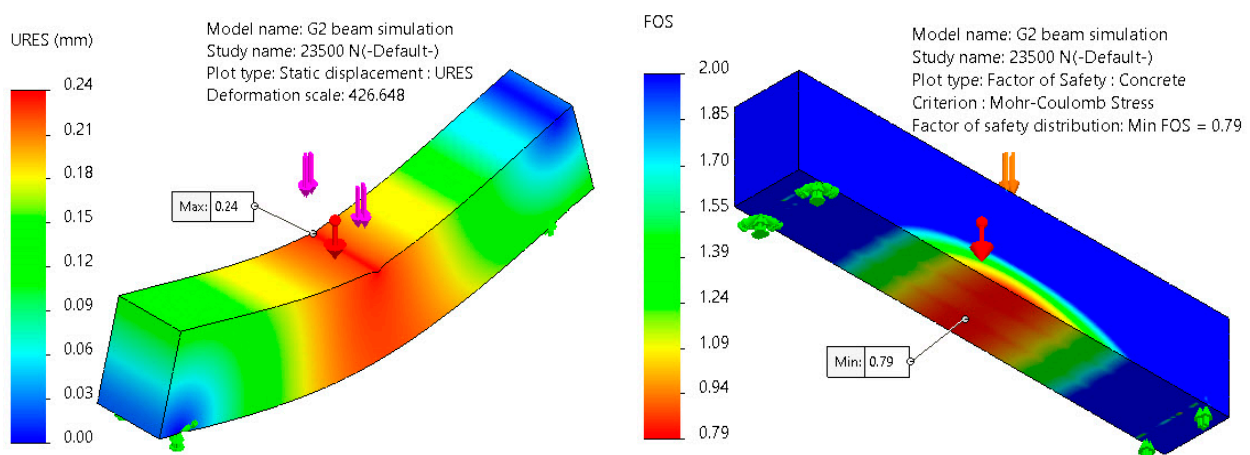
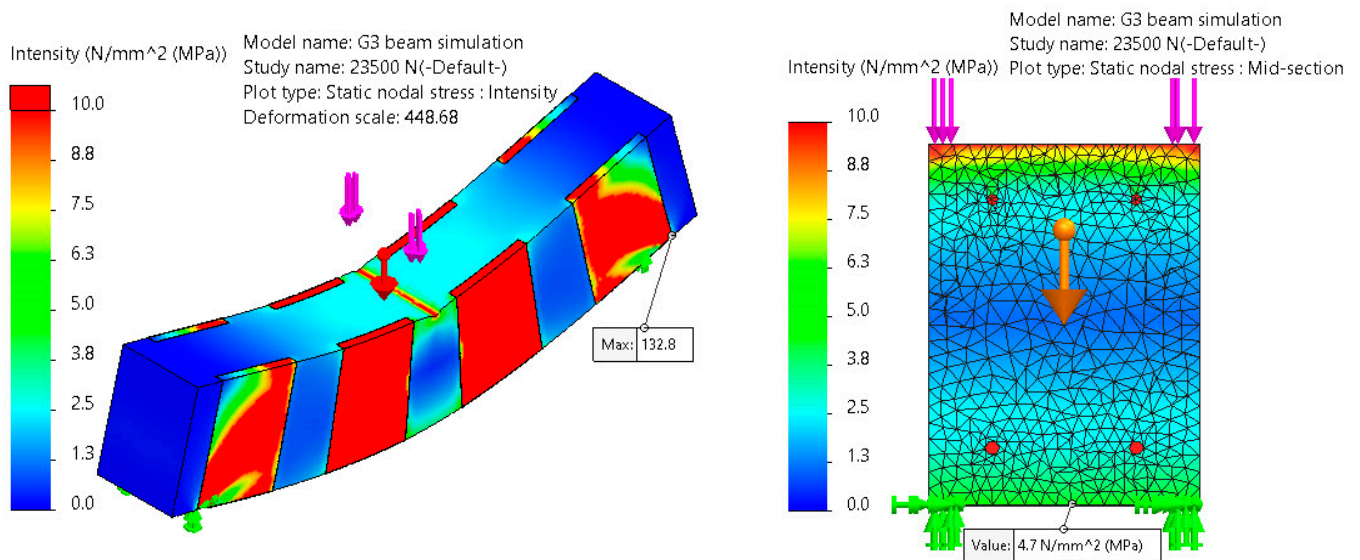


**Figure 14.** Deformed shape of the resultant displacement (URES) of G2 at 23.5 kN load (left); The FOS plot for the concrete on G2 at 23.5 kN load (right).

### 3.2.3. Simulation of the Beam G3 under the Load of 23.5 kN

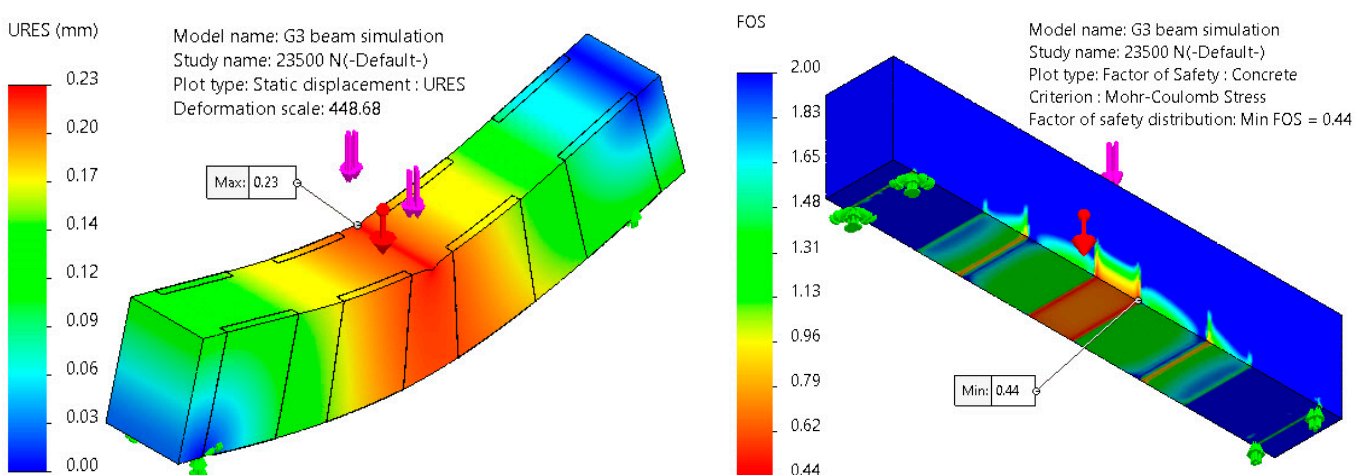
The G3 beam is coated with SikaWrap 230C mesh in four areas. The width of each coat is 150 mm, and the distance between wraps is 100 mm, according to Figure 5.

Figure 15(left) shows the stress intensity distribution on the beam and CFRP reinforcement elements. Figure 15(right) shows no modification of the stress intensity at the beam base with respect to G1 at the same place, the beam's center (Figure 11(right)).



**Figure 15.** Deformed plot (left) and mid-section representation (right) of the stress intensity of G3 at 23.5 kN load.

A stress reduction in G3 was not noticed compared to G1. So, the wrap presence did not reduce the stress, but considering the displacement reduction from 0.25 mm (Figure 12(left)) to 0.23 mm (Figure 16(left)), the beam body stability increased. The experiments conducted on G3 confirmed this finding; fewer visible cracks were observed in G3 compared to G1. From the viewpoint of FOS (Figure 16(right)), G3 is more susceptible to cracks than G1 in the uncovered zones with CFRP due to the concentrated stress at the wrap's boundary. We assume that microcracks exist but are not dangerous in this loading case.



**Figure 16.** Deformed shape of the resultant displacement (URES) of G3 at 23.5 kN load (left); The FOS plot for the concrete on G3 at 23.5 kN load (right).

### 3.2.4. Simulation of the Beam G3cw under the Load of 23.5 kN

The beam G3cw does not correspond to the experimental beams. The wrap arrangement, with a mesh at the middle, should increase the beam strength and reduce the crack initiation because the central wrap corresponds to the position of the maximum bending moment. Similar to the G3, the stress intensity distribution, the resultant displacement URES, and FOS graphs were plotted in Figures 17 and 18.

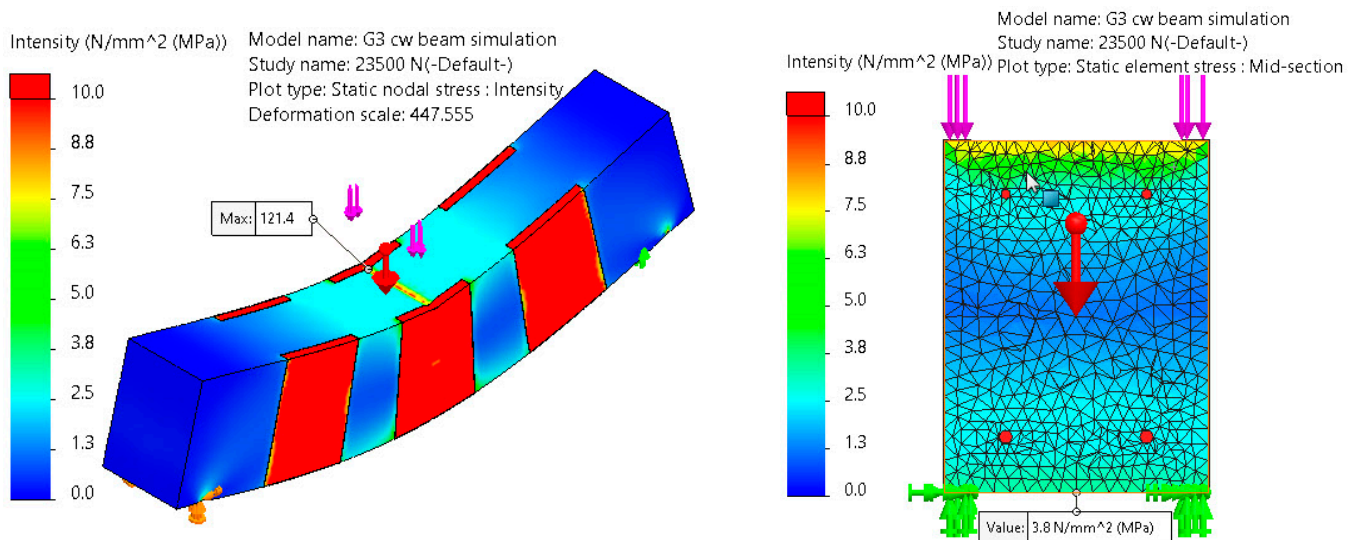


**Figure 17.** Deformed plot (left) and mid-section representation (right) of the stress intensity of G3cw at 23.5 kN load.

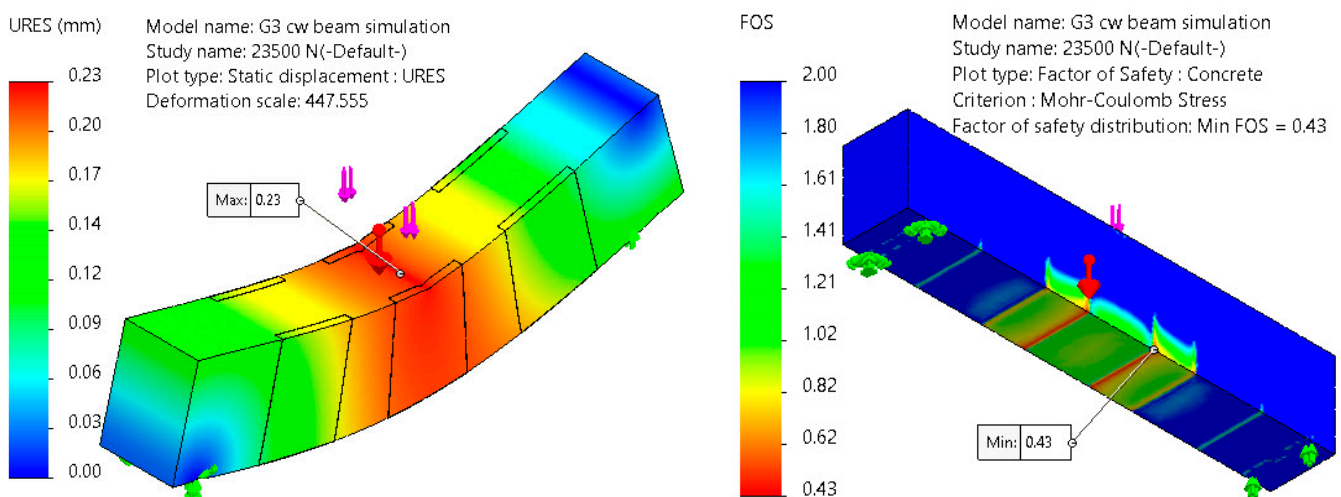


**Figure 18.** Deformed shape of the resultant displacement (URES) of G3cw at 23.5 kN load (left); The FOS plot for the concrete on G3cw at 23.5 kN load (right).

Comparison of G3 with G3cw shows that the stress intensity on the lower point of the beam and the resultant displacement URES remained the same (Figures 16 and 18). It can be concluded that different disposals of the wraps produce similar results.

### 3.2.5. Cumulative Results of the Simulations and Discussions

Similar experiments have been performed replacing 23.5 kN with 37.5 kN. Tables 4 and 5 contain the comparison of the obtained results during the simulations for both loading cases.

**Table 4.** The results for the load of 23.5 kN in the lower mid-beam.

	Values from Simulation				Reinforcement Effect (Reduction)		
	G1	G2	G3	G3cw	G2 vs. G1	G3 vs. G1	G3cw vs. G1
Mechanical properties							
Stress intensity (MPa)	4.70	4.60	3.80	3.80	2.1%	0.0%	19.1%
Displacement—URES (mm)	0.25	0.24	0.23	0.23	4.0%	8.0%	8.0%

**Table 5.** The results for the load of 37.5 kN in the lower mid-beam.

	Values from Simulations				Reinforcement Effect (Reduction)		
	G1	G2	G3	G3cw	G2 vs. G1	G3 vs. G1	G3cw vs. G1
Mechanical properties							
Stress intensity (MPa)	7.50	7.30	7.50	6.00	2.7%	0.0%	20.0%
Displacement—URES (mm)	0.40	0.38	0.36	0.37	5.0%	7.5%	9.0%

The simulation at 23.5 kN corresponds to the experimental results because the same deflection (0.25 mm) was obtained for the G1 beam. The calculated stress at this deflection does not damage the concrete beam. At higher stress values, the simulation cannot be compared with the experiments due to the cracks apparition, which cannot be simulated with SolidWorks. The only values that can be compared are the deflections until the cracks initiate.

The numerical results show a significant increase in strength for the beams G2 reinforced with CFRP materials. The G3 beam has a fiber coat instead of the lamella, and no stress intensity reduction was recorded while the deflection URES decreased. It is the consequence of the fiber reinforcement position. The CFRP reinforcing diminishes the URES in simulation and implicitly reduces the cracks in the experimental model, increasing the applied force. As the simulations cannot show the cracks that most influence concrete failure, the braking force cannot be determined this way. That is why the simulations have been performed at the same load, and stress intensity and displacement URES were compared. Analyzing the results of the G3cw simulation, we notice only changes in the deflection. This result gives an idea about the effect of the wraps bonded to the concrete beam. The concrete crack initiation is delayed, and its expansion is partially limited when using wraps. As a response to the applied force, the stress intensity remains at the same value. It can be considered that the beam becomes harder (surface stability) but not stronger (stiffness increases).

When we compare the simulation with the experiments, we get the same results for G2. However, the results differ for G3. The reason can be the wraps' setup, which makes identifying crack initiation and propagation in the experiments difficult.

To confirm the effect of the wrap, two supplementary stress intensity plots are provided for G3 and G3cw at 100 mm from the center of the beam (Figure 19).

The results from Table 6 show that the stress in the zones protected with CFRP wraps is lower than in the unprotected ones. For G3, the stress intensity is 4.7 MPa (in the unprotected zone), 20% higher than the 3.8 MPa found for G3cw (protected zone). Analogous, for G3, the stress intensity is 3.2 MPa (in a protected zone), 24% lower than 4.2 MPa found for G3cw (unprotected zone). Therefore, the covered areas are less susceptible to the cracks' apparition and propagation. The same conclusion was drawn after visual observation of the cracks on the beams during the experimental study.

**Table 6.** Comparison of Stress Intensity (MPa) of G3 and G3cw beams.

Location	G3	G3cw
The beam center	4.7	3.8
100 mm from the beam center	3.2	4.2

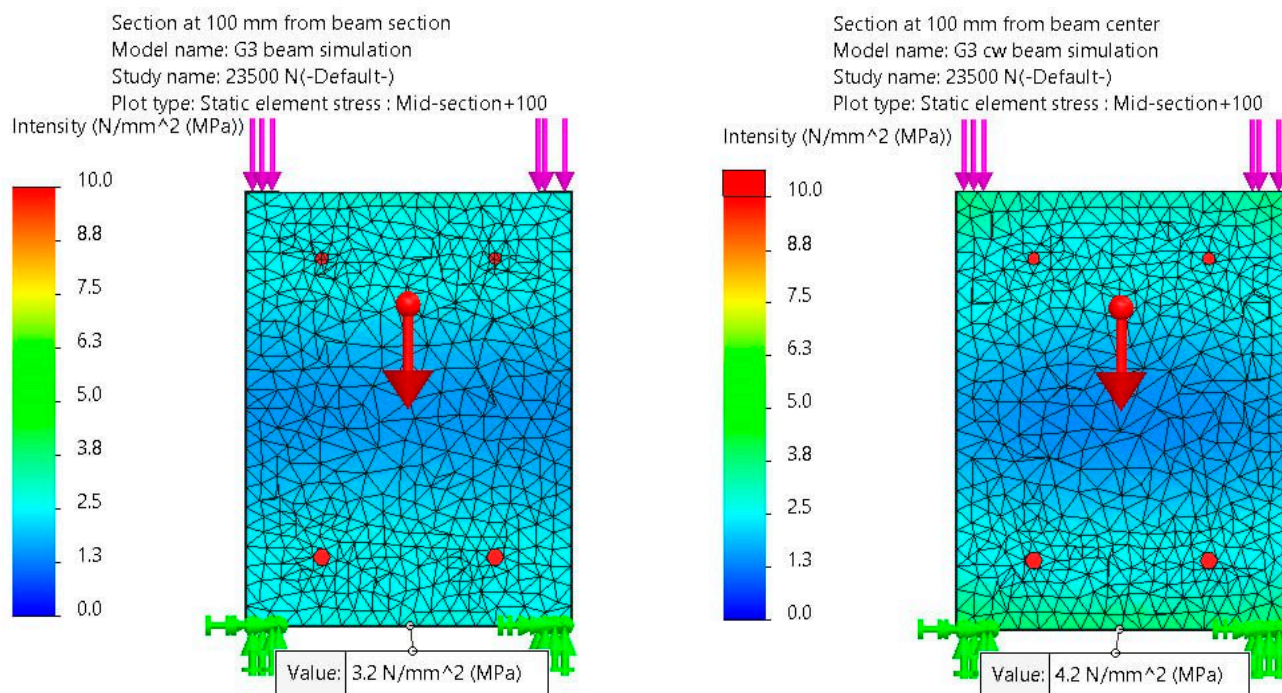


**Figure 19.** Mid-section representation of the stress intensity of (left) G3 and (right) G3cw at 23.5 kN load. A section at 100 mm from the beam center.

Studying the concrete structures' behavior under mechanical stress using FEA is not easy because all brittle materials (like concrete) suffer cracks that must be simulated. Another issue arises when different materials are used in the same simulation model. The materials with non-linear behavior must be defined in the software material library based on their stress–strain curve. If the software deals simultaneously with materials with linear and non-linear behavior, choosing the computational method and failure criterion may be difficult for designers. Finally, discretization is difficult when the simulation model comprises elements with tiny dimensions (as glue layers) and big-size ones.

The search of the scientific literature emphasized only a few articles that compare the experimental results on fiber-RC beams with the simulated ones, which might be due to the simulation complexity, even when using dedicated FEA software. Dedicated software may give an appropriate result that is close to the real behavior of a material or structure. Simulia Abacus or Ansys can provide a high degree of dispersion of results. Our investigations did not return CFRP RC analyses using SolidWorks. From this point of view, this study provides new insights into the topic. Despite its shortcomings, the large utilization of SolidWorks in structural design and ease of use are advantages that should be considered.

Moreover, comparing the FEA software results with those obtained from experimental tests validates computational methods based on the Finite Element Method. Once the numerical method is defined, new studies can be developed without experimental testing.

The experimental results concord with those of other studies, indicating an increased beam resistance when using lamella or wraps (especially wraps) to consolidate the damaged structures. It was shown that utilizing CFRP materials improves the concrete compressive strength and ultimate strain [34]. The CFRP RC beams have a higher deflection and load-carrying capacity and increased corrosion resistance than those without cover, which augments the structures' durability [71–73].

From a practical viewpoint, CFRP can be utilized to confine concrete by retrofitting RC beams or columns with a jacket or using concrete tubes filled with carbon fiber polymers for new infrastructure projects. Their low weight is another advantage of CFRP use, together with the reductions of energy and material consumption that increases the structure's life in the actual sustainability effort. Still, CFRP composites can exhibit brittle behavior

and limited fire resistance. The sudden detaching of CPRP lamella and the peeling out of the wraps (when glued on the beam surface) are some of the significant challenges to be addressed [19].

#### 4. Conclusions

The main aim of this study was to compare the experimental results of the flexural behavior of CFRP beams with the simulated ones in three scenarios. Whereas many studies emphasized the advantages of reinforcing the beams using CFRP, only a few provided simulation results of the reinforced beams in different scenarios, and none used SolidWorks as a tool.

The simulations show a similar capacity of beam reinforcement with CFRP materials to that obtained in the experimental tests at 23.5 kN loading force. Therefore, simulations are safer from the viewpoint of the beam's final strength capacity and can be used in preliminary design if the computed stress values for concrete do not exceed 50% of the admissible value. The cracks apparition will change the beam behavior at higher stress, and the simulations will no longer be helpful.

Important aspects that will be further investigated are the optimum position of the CFRP reinforcement with respect to the loading cases and the clarification of the cracks' apparition in different scenarios. Although the CFRPs are mainly applied on the surfaces of the beams by gluing, mechanical or thermal methods should also be employed for this aim. Therefore, different solutions for obtaining the reinforced beams' best mechanical behavior will also be investigated.

**Author Contributions:** Conceptualization, C.E.C.; methodology, C.E.C., C.Ş.D. and A.B.; software, C.Ş.D.; validation, C.Ş.D. and A.B.; formal analysis, C.Ş.D. and A.B.; investigation, C.E.C., C.Ş.D. and A.B.; resources, C.Ş.D. and A.B.; data curation, C.Ş.D.; writing—original draft preparation, C.E.C., C.Ş.D. and A.B.; writing—review and editing, A.B. and C.Ş.D.; visualization, C.Ş.D.; supervision, A.B.; project administration, A.B.; funding acquisition, A.B. All authors have read and agreed to the published version of the manuscript.

**Funding:** This research received no external funding.

**Institutional Review Board Statement:** Not applicable.

**Informed Consent Statement:** Not applicable.

**Data Availability Statement:** Data will be available on request from the first author.

**Conflicts of Interest:** The authors declare no conflict of interest.

#### Nomenclature

AE	Acoustic emission
CAE	Computer-Aided Engineering. It encompasses some of the computer software. CAE refers to any computer software that aids in engineering, analysis, and manufacturing tasks.
CAD	Computer-Aided Design
CFRP	Carbon fibre-reinforced polymers
FOS	Factor of Safety
$f_{ck}$	Characteristic cylinder compressive strength, 16 MPa
$f_{ck, cube}$	Characteristic cube compressive strength, 20 MPa
FRP	Fibre-reinforced polymers
NDTs	Non-destructive evaluation techniques
RC	Reinforced concrete
URES	Resultant displacement

#### References

1. Tan, K.H. Fibre-Reinforced Polymer Reinforcement for Concrete Structures. In Proceedings of the Sixth International Symposium on FRP Reinforcement for Concrete Structures (FRPRCS-6), Singapore, 8–10 July 2003. 1253p. [\[CrossRef\]](#)

2. EMPA. Materials Science and Technology. Available online: <https://www.empa.ch/web/s604/brueckenpionier-urs-meier> (accessed on 22 February 2024).
3. Kossakowski, P.G.; Wciślik, W. Fiber-Reinforced Polymer Composites in the Construction of Bridges: Opportunities, Problems and Challenges. *Fibers* **2022**, *10*, 37. [[CrossRef](#)]
4. Chróścielewski, J.; Miśkiewicz, M.; Pyrzowski, Ł.; Sobczyk, B.; Wilde, K. A novel sandwich footbridge—Practical application of laminated composites in bridge design and in situ measurements of static response. *Comp. Part B* **2017**, *126*, 153–161. [[CrossRef](#)]
5. Phillis, S.E.; Parretti, R.; Nanni, A. *Evaluation of FRP Repair Method for Cracked Bridge Members*; Center for Infrastructure Engineering Studies, University of Missouri: Rolla, MO, USA, 2004.
6. Siwowski, T.; Zobel, H.; Al-Khafaji, T.; Karwowski, W. FRP bridges in Poland: State of practice. *Arch. Civ. Eng.* **2021**, *67*, 5–27.
7. Sonnenschein, R.; Gajdosova, K.; Holly, I. FRP composites and their using in the construction of bridges. *Proc. Eng.* **2016**, *161*, 477–482. [[CrossRef](#)]
8. Vovesný, M.; Rotter, T. GFRP bridge deck panel. *Proc. Eng.* **2012**, *40*, 492–497. [[CrossRef](#)]
9. Taerwe, L.R.; Matthys, S. FRP for concrete constructions. *Concr. Int.* **1999**, *21*, 33–36.
10. *TR 50 Guide to Surface Treatments for Protection and Enhancement of Concrete*; Concrete Society: Blackwater, UK, 1997; Available online: <https://www.thenbs.com/PublicationIndex/documents/details?Pub=CS&DocID=249194> (accessed on 20 January 2024).
11. TGU 3 Use of Fibre Composites in Concrete Bridges—State of the Art Review. 2000. Available online: <https://www.thenbs.com/PublicationIndex/documents/details?Pub=CBDG&DocID=254886> (accessed on 20 January 2024).
12. *TR 55 Design Guidance for Strengthening Concrete Structures Using Fibre Composite Materials*, 3rd ed.; Concrete Society: Blackwater, UK, 2012; Available online: <https://www.thenbs.com/PublicationIndex/documents/details?Pub=CS&DocID=305394> (accessed on 20 January 2024).
13. *Guide for the Design and Construction of Externally Bonded FRP Systems for Strengthening Concrete Structures*; American Concrete Institute: Farmington Hills, MI, USA, 2017. Available online: [https://afzir.com/knowledge/wp-content/uploads/2018/03/ACI\\_440\\_2R\\_17\\_Guide\\_for\\_the\\_Design.pdf](https://afzir.com/knowledge/wp-content/uploads/2018/03/ACI_440_2R_17_Guide_for_the_Design.pdf) (accessed on 26 January 2024).
14. C149-1987; Technical Instructions on Defect Repair Procedures for Concrete and Reinforced Concrete Elements. MATRIXROM: Bucharest, Romania, 2017. (In Romanian)
15. *GP 033-1998*; Design and Execution Guide for Carrying out Interventions with Reinforced Polymer Concrete on Reinforced Concrete Elements Degraded by Corrosion. Available online: <https://tkobra.ro/blog/2017/11/28/ghid-de-proiectare-sl-executie-pentru-realizarea-interventiilor-cu-betoane-polimerice-armate-la-elemente-din-beton-armat-degradate-prin-coroziune/> (accessed on 2 February 2024). (In Romanian)
16. INCERC, ST.050-2006, Technical Specification Regarding the Use of Polymer Adhesives in Construction. Available online: [https://www.mdtpa.ro/userfiles/reglementari/Domeniul\\_XV/15\\_15\\_ST\\_050\\_2006.pdf](https://www.mdtpa.ro/userfiles/reglementari/Domeniul_XV/15_15_ST_050_2006.pdf) (accessed on 2 February 2024). (In Romanian)
17. INCERC, Normative Regarding Fiber Reinforcement of Concrete Structural Elements. 22 June 2004. Available online: <https://lege5.ro/Gratuit/heztqmbms/reglementarea-tehnica-normativ-privind-consolidarea-cu-fibre-a-elementelor-structurale-de-beton-din-22062004> (accessed on 2 February 2024). (In Romanian)
18. Ur Rehman Khan, A.; Fareeda, S. Behaviour of Reinforced Concrete Beams Strengthened by CFRP Wraps with and without End Anchorages. *Proc. Eng.* **2014**, *77*, 123–130. [[CrossRef](#)]
19. Saleem, M.U.; Qureshi, H.J.; Amin, M.N.; Khan, K.; Khurshid, H. Cracking Behavior of RC Beams Strengthened with Different Amounts and Layouts of CFRP. *Appl. Sci.* **2019**, *9*, 1017. [[CrossRef](#)]
20. Zhong, J.; Zhuang, H.; Shiyang, P.; Zhou, M. Experimental and numerical analysis of crack propagation in reinforced concrete structures using a three-phase concrete model. *Structures* **2021**, *33*, 1705–1714. [[CrossRef](#)]
21. Arduini, M.; Nanni, A. Behaviour of precracked RC beams strengthened with carbon FRP sheets. *J. Compos. Constr.* **1997**, *1*, 63–73. [[CrossRef](#)]
22. Bu, J.; Chen, H.; Hu, L.; Yang, H.; Liu, S. Experimental Study on Crack Propagation of Concrete Under Various Loading Rates with Digital Image Correlation Method. *Int. J. Concr. Struct. Mater.* **2020**, *14*, 25. [[CrossRef](#)]
23. Ding, J.; Wang, F.; Huang, X.; Chen, S. The Effect of CFRP Length on the Failure Mode of Strengthened Concrete Beams. *Polymers* **2014**, *6*, 1705–1726. [[CrossRef](#)]
24. Kim, S.-W.; Kim, K.-H. Prediction of Deflection of Reinforced Concrete Beams Considering Shear Effect. *Materials* **2021**, *14*, 6684. [[CrossRef](#)] [[PubMed](#)]
25. Kalkan, I. Deflection Prediction for Reinforced Concrete Beams Through Different Effective Moment of Inertia Expressions. *Int. J. Eng. Res. Dev.* **2013**, *5*, 1. Available online: <https://dergipark.org.tr/tr/download/article-file/353723> (accessed on 2 March 2024).
26. Slaitas, J.; Daugevičius, M.; Valivonis, J.; Grigorjeva, T. Crack Width and Load-Carrying Capacity of RC Elements Strengthened with FRP. *Int. J. Polymer Sci.* **2018**, *2018*, 274287. [[CrossRef](#)]
27. Lin, G.; Yu, T.; Teng, J.G. Design-Oriented Stress–Strain Model for Concrete under Combined FRP-Steel Confinement. *J. Compos. Constr.* **2016**, *29*, 04015084. [[CrossRef](#)]
28. Lam, L.; Teng, J.G. Design-oriented stress–strain model for FRP-confined concrete. *Constr. Build. Mater.* **2003**, *17*, 471–489. [[CrossRef](#)]
29. Megalooikonomou, K.G.; Papavasileiou, G.S. Analytical Stress-Strain Model for FRP-Confined Rectangular RC Columns. *Front. Built Environ. Earthq. Eng.* **2019**, *5*, 39. [[CrossRef](#)]

30. Li, K.; Zhao, D.; Wang, X.; Feng, H.; Zou, X. Investigation of crack growth in CFRP-concrete interface under fatigue loading. *Structures* **2021**, *34*, 356–367. [[CrossRef](#)]
31. Uz, M.E.; Guner, Y.; Avci, E. Strengthening of Reinforced Concrete Beams via CFRP Orientation. *Buildings* **2024**, *14*, 82. [[CrossRef](#)]
32. Al-Jasmi, S.; Ariffin, N.F.; Seman, M.A. Model analysis of carbon fiber reinforcement properties for reinforced concrete beams to resist blast loads. *Mater. Today Proc.* **2023**, *in press*. [[CrossRef](#)]
33. Carvalho Silva, R.J.; Bezerra Cabral, A.E.; da Silva Júnior, F.E.S.; de Vasconcelos Filho, J.L.; Farias Eugênio, D.E. Analysis of reinforced concrete beams strengthened with different CFRP lengths. *Acta Sci. Technol.* **2020**, *42*, e44212. [[CrossRef](#)]
34. Teng, J.G.; Chen, J.F.; Smith, S.T.; Lam, L. Behaviour and strength of FRP-strengthened RC structures: A state-of-the-art. *Proc. Inst. Civ. Eng. Struct. Build.* **2003**, *156*, 51–62. [[CrossRef](#)]
35. Pawlak, A.M.; Górný, T.; Dopierała, Ł.; Paczos, P. The Use of CFRP for Structural Reinforcement—Literature Review. *Metals* **2023**, *12*, 1470. [[CrossRef](#)]
36. Mpalaskas, A.C.; Matikas, T.E.; Aggelis, D.G. 13—Acoustic monitoring for the evaluation of concrete structures and materials. In *Acoustic Emission and Related Non-Destructive Evaluation Techniques in the Fracture Mechanics of Concrete*, 2nd ed.; Ohtsu, M., Ed.; Woodhead Publishing: Cambridge, UK, 2021; pp. 257–280.
37. Papadopoulos, N.A.; Naoum, M.C.; Sapidis, G.M.; Chalioris, C.E. Cracking and Fiber Debonding Identification of Concrete Deep Beams Reinforced with C-FRP Ropes against Shear Using a Real-Time Monitoring System. *Polymers* **2023**, *15*, 473. [[CrossRef](#)]
38. Maierhofer, C.; Kohl, C.; Wöstmann, J. 5—Combining the results of various non-destructive evaluation techniques for reinforced concrete: Data fusion. In *Non-Destructive Evaluation of Reinforced Concrete Structures*; Maierhofer, C., Reinhardt, H.-W., Dobmann, G., Eds.; Woodhead Publishing: Cambridge, UK, 2010; Volume 2, pp. 95–107.
39. Shull, P.J. *Nondestructive Evaluation: Theory, Techniques, and Applications*; Marcel Dekker: New York, NY, USA, 2002.
40. Gunes, O. 5—Failure modes in structural applications of fiber-reinforced polymer (FRP) composites and their prevention. In *Developments in Fiber-Reinforced Polymer (FRP) Composites for Civil Engineering*; Uddin, N., Ed.; Woodhead Publishing: Cambridge, UK, 2013; pp. 115–147.
41. Wang, B.; Zhong, S.; Lee, T.-L.; Fancey, K.S.; Mi, J. Non-destructive Testing and Evaluation of Composite Materials and Structures—Review. *Adv. Mech. Eng.* **2020**, *12*, 1687814020913761. [[CrossRef](#)]
42. Grosse, C.U.; Ohtsu, M. *Acoustic Emission Testing*; Springer: Berlin, Germany, 2010.
43. Hung, Y.Y.; Chen, Y.S.; Ng, S.P.; Liu, L.; Huang, Y.H.; Luk, B.L.; Ip, R.W.L.; Wu, C.M.L.; Chung, P.S. Review and comparison of shearography and active thermography for nondestructive evaluation. *Mater. Sci. Eng. R Rep.* **2009**, *64*, 73–112. [[CrossRef](#)]
44. Yu, T.-Y.; Büyükköztürk, O. A far-field airborne radar NDT technique for detecting debonding in GFRP-retrofitted concrete structures. *NDT E. Int.* **2008**, *41*, 10–24. [[CrossRef](#)]
45. Alves, C.L.; Oliveira, J.S.; Tannus, A.; Tarpani, A.C.S.P.; Tarpani, J.R. Detection and Imaging of Damages and Defects in Fibre-Reinforced Composites by Magnetic Resonance Technique. *Materials* **2021**, *14*, 977. [[CrossRef](#)]
46. Shen, J.; Arruda, M.R.T.; Pagani, A. Concrete damage analysis based on higher-order beam theories using fracture energy regularization. *Mech. Adv. Mater. Struct.* **2023**, *30*, 4582–4596. [[CrossRef](#)] [[PubMed](#)]
47. Ziehl, P.; ElBatanouny, M. 11—Low-level acoustic emission in the long-term monitoring of concrete. In *Acoustic Emission and Related Non-Destructive Evaluation Techniques in the Fracture Mechanics of Concrete*, 2nd ed.; Ohtsu, M., Ed.; Woodhead Publishing: Cambridge, UK, 2015; pp. 205–224.
48. Maierhofer, C.; Reinhardt, H.-W.; Dobmann, G. *Non-Destructive Evaluation of Reinforced Concrete Structures, Vol. 1: Deterioration Processes and Standard Test Methods*; CRC Press: Boca Raton, FL, USA; Woodhead Publishing: Cambridge, UK, 2010.
49. Karbhari, V.M.; Kaiser, H.; Navada, R.; Ghosh, K.; Lee, L. Methods for Detecting Defects in Composite Rehabilitated Concrete Structures. Final Report, SPR 336. 2005. Available online: [https://www.oregon.gov/odot/Programs/ResearchDocuments/Detect\\_Defects\\_Comp\\_Structures.pdf](https://www.oregon.gov/odot/Programs/ResearchDocuments/Detect_Defects_Comp_Structures.pdf) (accessed on 3 March 2024).
50. Ohtsu, M. *Acoustic Emission and Related Non-Destructive Evaluation Techniques in the Fracture Mechanics of Concrete*, 2nd ed.; Woodhead Publishing: Cambridge, UK, 2015.
51. Kong, Y.; Bennett, C.J.; Hyde, C.J. A review of non-destructive testing techniques for the in-situ investigation of fretting fatigue cracks. *Mater. Des.* **2020**, *196*, 109093. [[CrossRef](#)]
52. Gheorghiu, C. A Study on the Behavior of RC Beams Reinforced with CFRP Composite Materials. Ph.D. Thesis, Transilvania University of Brasov, Braşov, Romania, 2011.
53. Cazacu, C.; Dobrovolschi, M. *Methodologies Involving the Strengthening of Concrete Elements Using Fiber-Reinforced Polymers*; Transilvania University of Braşov: Braşov, Romania, 2011.
54. Cazacu, C.; Muntean, R. Crack widths in RC beams externally bonded with CFRP sheets and plates. *J. Appl. Eng. Sci.* **2011**, *1*, 19–26.
55. Cazacu, C.; Muntean, R. Tests on RC beams strengthened in flexure with glued CFRP strips and fabrics. *J. Appl. Eng. Sci.* **2013**, *3*, 15–20.
56. Cazacu, C.; Gălăţanu, T.; Mizgan, P.; Muntean, R.; Tamas, F. Experimental research in flexural behavior of carbon fiber polymer strengthened beams. *Proc. Eng.* **2017**, *181*, 257–264. [[CrossRef](#)]
57. EN 12390-5:2019; Testing Hardened Concrete—Part 5: Flexural Strength of Test Specimens. iTeh, Inc.: Newark, DE, USA, 2019. Available online: <https://standards.iteh.ai/catalog/standards/cen/5653c2c7-55a9-4bcb-8e13-5b1dfb0e3baf/en-12390-5-2019> (accessed on 23 November 2023).

58. Annex to the Order of the Minister of Regional Development and Tourism No. 2.514/2010 for the Approval of the Technical Regulation “Regulations for the Production and Execution of Works of Concrete, Reinforced Concrete and Prestressed Concrete—Part 2: Execution of Concrete Works”, Indicative NE 012/2-2010. Official Monitor of Romania, Part I, Year 178 (XXII)—Nr. 853 Bis, Monday, 20 December 2010. Available online: <https://colegiu-diriginti-santier.ro/norme/NE-012-2-2010%20102%20normativ%20executare%20lucrari%20beton%20armat.pdf> (accessed on 10 November 2023). (In Romanian)
59. SR EN 206-1:2002; Concrete: Part 1: Specification, Performance, Production and Conformity. Available online: <https://toaz.info/doc-view> (accessed on 10 December 2023). (In Romanian)
60. SikaWrap®-230 C. Available online: <https://rou.sika.com/ro/solutii-pentru-constructii/repara/consolidare-structurala/consolidare-pe-bazadefibradecarbon/sikawrap-230-c.html> (accessed on 10 December 2023). (In Romanian)
61. Sikadur®-330. Available online: <https://usa.sika.com/en/construction/repair-protection/structural-strengthening/epoxies/sikadur-330.html> (accessed on 10 December 2023).
62. Sika Carbodur Carbon Fiber Strips S1012. Available online: <https://www.indconsupply.com/sika-carbodur-carbon-fiber-strips-s1012> (accessed on 10 December 2023).
63. Sikadur®-30. Available online: <https://gbr.sika.com/en/construction/structural-strengthening/adhesives-and-bonding/structural-adhesives/sikadur-30.html> (accessed on 10 November 2023).
64. Eurocode 2: Design of Concrete Structures. Available online: <https://eurocodes.jrc.ec.europa.eu/EN-Eurocodes/eurocode-2-design-concrete-structures> (accessed on 10 December 2023).
65. SOLIDWORKS 2022—Simulation. Available online: <https://www.solidworks.com/media/solidworks-2022-simulation> (accessed on 30 January 2024).
66. Mohr-Coulomb Stress Criterion. Available online: [https://help.solidworks.com/2022/english/Solidworks/cworks/r\\_Mohr-Couomb\\_Stress\\_Criterion.htm?rid=20046](https://help.solidworks.com/2022/english/Solidworks/cworks/r_Mohr-Couomb_Stress_Criterion.htm?rid=20046) (accessed on 30 November 2023).
67. Maximum Share Stress. Available online: [https://help.solidworks.com/2024/English/SolidWorks/cworks/r\\_Maximum\\_Shear\\_Stress\\_Criterion.htm](https://help.solidworks.com/2024/English/SolidWorks/cworks/r_Maximum_Shear_Stress_Criterion.htm) (accessed on 30 January 2024).
68. Daugevičius, M.; Valivonis, J.; Skuturna, T. Prediction of Deflection of Reinforced Concrete Beams Strengthened with Fiber Reinforced Polymer. *Materials* **2019**, *12*, 1367. [CrossRef] [PubMed]
69. Suidan, M.; Schnobrich, W.C. Finite element analysis of reinforced concrete. *J. Struct. Div.* **1973**, *99*, 2109–2122. [CrossRef]
70. Bangash, M.Y.H. *Concrete and Concrete Structures: Numerical Modelling and Application*; Elsevier Applied Science: London, UK, 1989.
71. Ozturk, M.; Sengun, K.; Arslan, G. CFRP Contribution to Load-Carrying Capacity of Retrofitted Geopolymer Concrete Beams. *Structures* **2023**, *48*, 1391–1402. [CrossRef]
72. Vijayan, D.S.; Sivasuriyan, A.; Devarajan, P.; Stefańska, A.; Wodzyński, Ł.; Koda, E. Carbon Fibre-Reinforced Polymer (CFRP) Composites in Civil Engineering Application—A Comprehensive Review. *Buildings* **2023**, *13*, 1509. [CrossRef]
73. Deng, J.; Eisenhauer Tanner, J.; Mukai, D.; Hamilton, H.R.; Dolan, C.W. Durability Performance of Carbon Fiber-Reinforced Polymer in Repair/Strengthening of Concrete Beams. *Mater. J.* **2015**, *112*, 247–258. [CrossRef]

**Disclaimer/Publisher’s Note:** The statements, opinions and data contained in all publications are solely those of the individual author(s) and contributor(s) and not of MDPI and/or the editor(s). MDPI and/or the editor(s) disclaim responsibility for any injury to people or property resulting from any ideas, methods, instructions or products referred to in the content.